

# User Separation for OFDMA Uplink

Mustafa E. Şahin\*, Ismail Guvenc‡, Moo-Ryong Jeong‡, and Hüseyin Arslan\*

\*Dept. of Electrical Engineering, University of South Florida, Tampa, FL, 33620

‡DOCOMO Communications Laboratories USA, Inc., 3240 Hillview Avenue, Palo Alto, CA, 94304

E-mail: msahin@mail.usf.edu, {iguvenc, jeong}@docomolabs-usa.com, arslan@eng.usf.edu

**Abstract**— Separating user signals in the uplink (UL) of an orthogonal frequency division multiple access (OFDMA) system without access to the subcarrier assignment scheme (SAS) is a challenging task, but it can have a number of useful applications. In this paper, a semi-blind user separation algorithm is proposed, which assumes time synchronization and availability of information on the type of SAS used. The proposed algorithm estimates the carrier frequency offsets and time delays of each frequency allocation block by exploiting the cross-correlations over pilot subcarriers. A clustering method to group the blocks is employed, where each group belongs to a different user. Mathematical model of the proposed algorithm is presented, and possible user separation applications in OFDMA-based femtocells are discussed. Feasibility of the algorithm is proved through practical simulations.

**Index Terms**— Carrier frequency offset estimation, cognitive radio, delay estimation, femtocell, OFDMA, user separation.

## I. INTRODUCTION

The uplink (UL) of orthogonal frequency division multiple access (OFDMA) systems poses a number of challenges that do not exist in the downlink (DL) due to the involvement of multiple users. Most of these problems including multiuser channel estimation [1], carrier frequency offset (CFO) estimation [2], synchronization and symbol timing estimation [3], [4], multiuser interference cancellation [5], and subcarrier and power allocation [6] are investigated extensively in the prior-art. However, the problem of separating UL user signals without access to the subcarrier assignment scheme (SAS) has not been investigated in detail in the literature, which may have interesting applications.

User separation in UL-OFDMA might be attractive for military communications, where it may be used for purposes such as eavesdropping. Another real-world scenario where user separation might be quite useful is a cochannel femtocell coexisting with a macrocell network, both of which have an OFDMA based physical layer. Assuming that the coexistence is based on a shared spectrum approach where the femtocell utilizes the available parts of the macrocell spectrum in an opportunistic manner, user separation can be very beneficial to the femtocell as discussed in detail in Section IV.

User separation in UL-OFDMA was considered in [7] for interleaved OFDMA systems. In [7], subcarriers allocated to different users follow a certain periodic structure, which leads to a user specific CFO. Hence, by estimating the CFOs, different user signals are identified and separated. In this paper, however, we propose a semi-blind user separation algorithm that can be applied to any SAS, which does not necessarily involve any periodicity.

Distinguishing between user signals can be accomplished utilizing various user-dependent signal features such as carrier frequency offsets, delays, energy levels, or certain user-specific parameters. The user separation algorithm considered in this

paper is based on exploiting the differences in user CFOs and delays.

In any OFDMA system, the subcarriers are allocated to users according to a certain SAS. The smallest allocation unit, which we will generically call a *block*, might be a *tile* in an 802.16e Partial Usage of Subchannels (PUSC) system or a *bin* in an 802.16e Adaptive Modulation and Coding (AMC) system. The user separation algorithm proposed in this paper assumes time synchronization to the UL signal and availability of information on the type of SAS used. It estimates the CFOs and delays for each block separately by performing cross-correlations over pilot subcarriers, and groups the blocks in the UL symbol according to their CFOs and delays using a clustering method. This way, it is able to determine how many UL users there are and to separate their subcarriers.

The organization of the paper is as follows. Section II provides the OFDMA system model. In Section III, a mathematical model of the proposed user separation algorithm is given. In Section IV, examples of user separation applications in femtocells are discussed. Simulation results are presented in Section V, and Section VI concludes the paper.

## II. OFDMA SYSTEM MODEL

Consider an OFDMA system with  $N_u$  users in the uplink. The sampled time domain signal at the transmitter of user  $i$  can be written as

$$x^{(i)}(n) = \sqrt{E_{tx,i}} \sum_{k \in \Gamma_i} X^{(i)}(k) e^{j2\pi kn/N}, -N_{CP} \leq n \leq N-1, \quad (1)$$

where  $E_{tx,i}$  is the total transmitted energy per symbol for user  $i$ ,  $\Gamma_i$  is the set of subcarriers with  $N_i$  elements assigned to user  $i$  out of  $N$  total subcarriers,  $k \in \Gamma_i$  is the subcarrier index,  $N_{CP}$  is the length of the cyclic prefix (CP), and  $X^{(i)}(k)$  is the data on the  $k$ th subcarrier of  $i$ th user.

A received symbol of user  $i$  after the FFT operation can be denoted as

$$\begin{aligned} R^{(i)}(k) &= X^{(i)}(k) H^{(i)}(k) e^{-j2\pi k \tau_i/N} e^{j\pi \xi_i} \text{sinc}(\pi \xi_i) \\ &\quad \times e^{j\pi k \delta_i} \text{sinc}(\pi k \delta_i) e^{j\Phi_i} + I^{(i)}(k) + W(k), \end{aligned} \quad (2)$$

where  $\xi_i$  is the carrier frequency offset (normalized by the subcarrier spacing  $f_s/N$ , where  $f_s$  is the sampling frequency),  $\delta_i$  is the sampling clock error,  $\tau_i$  is the timing offset of user  $i$ ,  $\Phi_i$  is the random phase noise caused by the instability of user  $i$ 's oscillator,  $H^{(i)}(k)$  is the frequency selective channel of user  $i$ ,  $I^{(i)}(k)$  is the inter-carrier interference (ICI) of user  $i$ , and  $W(k)$  is complex additive white Gaussian noise (AWGN). In the remainder of this paper, it will be assumed that the random phase noise as well as the sampling clock error in (2) are negligible.

From (2), it is seen that the CFO has two effects on the received signal. First, it results in amplitude degradation and a constant phase shift, and second, in ICI. Another effect, which becomes apparent when the phases of identical pilot subcarriers in two adjacent symbols are compared [8], is a phase shift that changes linearly over symbols. Taking this linear phase shift into account, the received signal over multiple symbols can be modeled as

$$\begin{aligned} Y^{(i)}(m, k) &= R^{(i)}(m, k)e^{j2\pi m\xi_i(1+\frac{N_{CP}}{N})} + W(m, k) \\ &= [X^{(i)}(m, k)H^{(i)}(m, k)e^{j\pi\xi_i}\text{sinc}(\pi\xi_i) \\ &\quad \times e^{-j2\pi k\tau_i/N} + I^{(i)}(m, k)]e^{j2\pi m\xi_i(1+\frac{N_{CP}}{N})} \\ &\quad + W(m, k), \end{aligned} \quad (3)$$

where  $m$  is the symbol index.

### III. USER SEPARATION METHOD

The proposed user separation method is based on exploiting the differences in the  $\tau_i$ 's and  $\xi_i$ 's of different UL-OFDMA users. It is assumed that the fundamental system parameters of the OFDMA system such as the SAS,  $N$ ,  $N_{CP}$ , and  $f_s$  are known by the UL receiver.

The UL-OFDMA signal is composed of independent frequency allocation blocks such as bins or tiles as shown in Fig. 1 for the 802.16e WiMAX UL-PUSC system. A certain user may use a number of these (not necessarily adjacent) blocks in the UL, depending on its data rate requirements and scheduling information. The first step of the proposed user separation method is to determine the occupied blocks via energy detection. Then, for each occupied block, the UL receiver performs  $\tau$  and  $\xi$  estimation. Next, occupied blocks are clustered according to their  $\tau$  and  $\xi$  values, where each

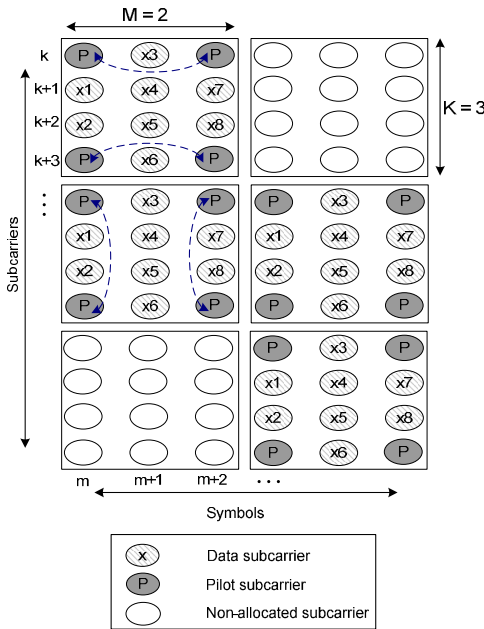


Fig. 1. 6 blocks in a WiMAX UL-PUSC system, where each block is a 4x3 tile, i.e.,  $K=3$  and  $M=2$ . Correlations for obtaining  $\hat{\xi}$  are illustrated in the first block, while the correlations for obtaining  $\hat{\tau}$  are illustrated in the second block.

separate cluster yields the blocks that belong to a certain user. This way,  $\hat{\Gamma}_i$ , which is an estimate for  $\Gamma_i$ , is obtained for each user  $i$ .

The total energy of each block  $\mathcal{B}_j$  can be calculated as follows

$$\Psi(\mathcal{B}_j) = \sum_{(m,k) \in \mathcal{B}_j} |Y(m, k)|^2, \quad (4)$$

where  $\mathcal{B}_j$  denotes the set of subcarriers in the  $j$ th block. This energy value is input to an energy detector that employs a threshold  $T_{\text{thr}}$

$$\Psi(\mathcal{B}_j) \stackrel{H_1}{\geq} T_{\text{thr}}, \quad (5)$$

where hypothesis  $H_1$  implies that block  $\mathcal{B}_j$  is occupied, and hypothesis  $H_0$  implies that it is not. Details of energy detection in OFDMA-UL, such as optimizing  $T_{\text{thr}}$  can be found in [9]. Let  $\mathcal{B}$  denote the set of all the occupied blocks that satisfy the hypothesis  $H_1$  in (5). Then, for each block within  $\mathcal{B}$ , carrier frequency offset and delay estimations are performed.

Regarding the CFO estimation, an important observation from (3) is that the linear phase shift caused by the CFO affects both the desired signal and ICI the same way. Therefore, a reliable  $\xi$  estimate can be obtained by correlating two identical pilot symbols [8], or pilot subcarriers in different symbols. If  $\mu_j$  denotes the indices of symbols within  $\mathcal{B}_j$  that carry pilot subcarriers, and  $\Pi_{m,j}$  denotes the subcarrier indices of pilots in symbol  $m$  within  $\mathcal{B}_j$ , a  $\xi$  estimate for  $\mathcal{B}_j$ , which will be denoted as  $\hat{\xi}_j$ , can be obtained by performing pairwise correlation between  $\Pi_{m,j}$  in different symbols within  $\mathcal{B}_j$ , separated by  $M$  symbols. Ignoring the ICI and noise terms, this correlation would be as follows

$$\begin{aligned} r_j^{(\xi)}(M) &= \sum_{m,k} Y^*(m, k)Y(m+M, k), \quad m \in \mu_j, \quad k \in \Pi_{m,j}, \\ &= e^{j2\pi\xi M(1+\frac{N_{CP}}{N})} \\ &\quad \sum_{m,k} |X(m, k)|^2 H^*(m, k)H(m+M, k)\text{sinc}^2(\pi\xi), \end{aligned} \quad (6)$$

where symbol  $m+M$  is within  $\mathcal{B}_j$ .  $\hat{\xi}_j$  can then be obtained as

$$\hat{\xi}_j = \frac{\angle(r_j^{(\xi)}(M))}{2\pi M(1+\frac{N_{CP}}{N})}, \quad (7)$$

where

$$\angle(r_j^{(\xi)}(M)) = \tan^{-1}(\text{Im}[r_j^{(\xi)}(M)]/\text{Re}[r_j^{(\xi)}(M)]). \quad (8)$$

The timing offset causes a phase shift that changes linearly over the subcarriers, but is independent from the symbol index. If  $p_{k,j}$  denotes the subcarrier indices of pilots that are at the same subcarrier index  $k$  in different symbols within  $\mathcal{B}_j$ , a  $\tau$  estimate for  $\mathcal{B}_j$ , which will be denoted as  $\hat{\tau}_j$ , can be obtained by correlating pilots at different subcarrier indices separated

by  $K$  subcarriers as

$$\begin{aligned} r_j^{(\tau)}(K) &= \sum_{m,k} Y^*(m, k)Y(m, k+K), \quad m \in \boldsymbol{\mu}_j, \quad k \in \boldsymbol{p}_{k,j}, \\ &= e^{-j2\pi\tau K/N} \\ &\sum_{m,k} |X(m, k)|^2 H^*(m, k)H(m, k+K)\text{sinc}^2(\pi\xi), \end{aligned} \quad (9)$$

where subcarrier  $k+K$  is within  $\mathcal{B}_j$ . The  $\tau$  estimate for  $\mathcal{B}_j$  is obtained as follows

$$\hat{\tau}_j = \frac{\angle(r_j^{(\tau)}(K))}{-2\pi K/N}, \quad (10)$$

where

$$\angle(r_j^{(\tau)}(K)) = \tan^{-1}(\text{Im}[r_j^{(\tau)}(K)]/\text{Re}[r_j^{(\tau)}(K)]). \quad (11)$$

As seen from (6), an important condition necessary for  $\hat{\xi}_j$  to be reliable is that the channel can be considered constant during  $M$  symbols. Taking the WiMAX standard as a reference, Table-I [10] provides information about channel coherence times for two different frequency bands. Given that the WiMAX symbol duration is around 0.1 ms, the channel coherence time covers up to 20 symbols even at a speed of 100 km/h in the 5.8 GHz band. Similarly, for any typical OFDMA based standard, it can be expected that this channel constancy condition is met.

Equation (9) also introduces a similar requirement in the frequency dimension. A reliable  $\hat{\tau}_j$  can only be obtained if  $H_m(k)$  for pilots separated by  $K$  subcarriers are highly correlated. Although this condition is met for any  $K$  in a single tap channel, in a frequency selective channel,  $K$  is typically taken a small number (e.g., in the WiMAX UL-PUSC system  $K$  is defined as 3).

Once  $\hat{\xi}_j$ 's and  $\hat{\tau}_j$ 's are obtained for all elements of  $\mathcal{B}$ , the user separation algorithm requires that  $\mathcal{B}_j$ 's are clustered according to their  $\hat{\xi}_j$ 's and  $\hat{\tau}_j$ 's, taking both values into account simultaneously. Each separate cluster generated by the clustering algorithm corresponds to a different user  $i$  and yields its subcarrier allocation vector estimate  $\hat{\Gamma}_i$ .

Prior to applying the clustering algorithm, the sets of  $\hat{\xi}_j$ 's and  $\hat{\tau}_j$ 's, which will be denoted as  $\hat{\xi}$  and  $\hat{\tau}$ , respectively, are normalized. In particular, we apply the following normalizations:

$$\tilde{\xi} = \frac{\hat{\xi} - \min(\hat{\xi})}{\max(\hat{\xi}) - \min(\hat{\xi})}, \quad (12)$$

and

$$\tilde{\tau} = \frac{\hat{\tau} - \min(\hat{\tau})}{\max(\hat{\tau}) - \min(\hat{\tau})}, \quad (13)$$

TABLE I  
TYPICAL DOPPLER SPREADS AND COHERENCE TIMES FOR WiMAX

Carrier Freq.	Speed	Max. Doppler	Coherence Time
2.5 GHz	2 km/h	4.6 Hz	200 ms
2.5 GHz	45 km/h	104.2 Hz	10 ms
2.5 GHz	100 km/h	231.5 Hz	4 ms
5.8 GHz	2 km/h	10.7 Hz	93 ms
5.8 GHz	45 km/h	241.7 Hz	4 ms
5.8 GHz	100 km/h	537 Hz	2 ms

respectively, which map both  $\hat{\xi}$  and  $\hat{\tau}$  into the interval  $[0, 1]$ . Therefore, as shown in Fig. 2, the clustering is performed on a  $[0, 1] \times [0, 1]$  plane. This type of normalization is mandated by the fact that the range of numerical values for  $\hat{\tau}$  is wider than the range of  $\hat{\xi}$ 's by at least two orders of magnitude. In fact, clustering without normalization results in a user separation that is solely based on  $\hat{\tau}$  values<sup>1</sup>.

The clustering algorithm requires to optimize the ratio of cluster dimensions ( $D_{\tilde{\xi}}$  and  $D_{\tilde{\tau}}$ ) for the best performance, and this ratio ( $D_{\tilde{\xi}}/D_{\tilde{\tau}}$ ) needs to be determined in proportion to the ratio of variances of  $\tilde{\xi}_j$  and  $\tilde{\tau}_j$ , i.e.,  $(\sigma_{\tilde{\xi}_j}^2/\sigma_{\tilde{\tau}_j}^2)$ . The variances of  $\angle(r_j^{(\xi)}(M))$  and  $\angle(r_j^{(\tau)}(K))$ , which are key to  $\hat{\xi}_j$  and  $\hat{\tau}_j$ , are approximately the same since AWGN noise has a similar impact on both correlations. The variances of  $\tilde{\xi}_j$  and  $\tilde{\tau}_j$ , however, related as follows

$$\sigma_{\tilde{\xi}_j}^2 = \frac{\text{Var}(\angle(r^{(\tau)}(M)))}{\text{Var}(\angle(r^{(\xi)}(K)))} \sigma_{\tilde{\tau}_j}^2 = c(\mathbf{r}_\tau, \mathbf{r}_\xi) \sigma_{\tilde{\tau}_j}^2, \quad (14)$$

where  $\angle(r^{(\tau)}(M))$  and  $\angle(r^{(\xi)}(K))$  denote the sets of all  $\angle(r_j^{(\tau)}(M))$ 's and  $\angle(r_j^{(\xi)}(K))$ 's, respectively. The scaling factor  $c(\mathbf{r}_\tau, \mathbf{r}_\xi)$  is introduced for notational brevity and will be used to represent the ratio of variances in (14) in the remainder of this paper. (14) indicates that  $\sigma_{\tilde{\xi}_j}^2/\sigma_{\tilde{\tau}_j}^2$  can be found before performing clustering by simply calculating  $c(\mathbf{r}_\tau, \mathbf{r}_\xi)$ . An important assumption regarding (14) is that the  $\xi$  and  $\tau$  values of different users are uniformly spread within  $[\min(\xi), \max(\xi)]$  and  $[\min(\tau), \max(\tau)]$ , respectively.

The first output obtained from the clustering algorithm is an estimate for the number of users ( $\hat{N}_u$ ). Using the normalized estimates  $\tilde{\xi}$  and  $\tilde{\tau}$ ,  $\hat{N}_u$  is determined by finding the cluster centers through the subtractive clustering algorithm outlined in [11], [12], where the factor  $\sqrt{c(\mathbf{r}_\tau, \mathbf{r}_\xi)}$  is set as  $D_{\tilde{\xi}}/D_{\tilde{\tau}}$

<sup>1</sup>Computer simulations without applying any normalization resulted in poor user separation performances.

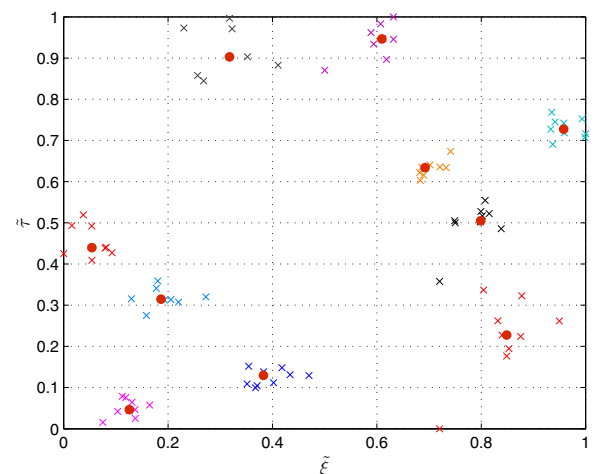


Fig. 2. Clusters on the  $\tilde{\tau}$  vs.  $\tilde{\xi}$  plane in a 10-user scenario (30 dB SNR is assumed for all user signals over MP channel).

for the potential clusters. In the next step, utilizing  $\hat{N}_u$ , the separation is performed via iterative partitioning algorithm discussed in [13], [14]. Iterative partitioning splits the input data into  $\hat{N}_u$  initial clusters. Then, for each cluster, it computes the sum of absolute distances from each point in the cluster to the cluster centroid, where the centroid is the component-wise median of the points in the cluster. By minimizing the total of these sums in an iterative manner, the clusters are determined.

A visual example that illustrates the clustering algorithm is provided in Fig. 2. It shows the clusters in a 10-user scenario, where signal-to-noise ratio (SNR) is assumed to be 30 dB for all user signals, and a multipath (MP) channel is considered. In Fig. 2, the large red dots constitute the cluster centers found through subtractive clustering, and the markers surrounding each of them indicate the blocks that belong to a certain user determined through iterative partitioning.

#### IV. USER SEPARATION APPLICATIONS FOR OFDMA BASED FEMTOCELLS

OFDMA based co-channel femtocells are systems where user separation can be useful in various ways. This section provides examples of practical applications related to femtocell-macrocell coexistence that can be realized when OFDMA based femtocells are equipped with the capability of separating the macrocell mobile station (mMS) signals in the uplink.

##### A. Classifying the Source of Co-channel Interference

The spectral occupancy that the femtocell base station (fBS) observes in the received uplink signal might be caused by mMSs or by other femtocells (fBSs or femtocell mobile stations (fMS)). Information about the source of this co-channel interference (CCI) can be beneficial to the fBS because if the occupant is another femtocell, it can negotiate sharing the occupied spectrum with that femtocell.

The CFO, delay, and power measurements performed for user separation can be utilized for classifying the source of CCI. Assuming that the mMSs will possibly have a high mobility, while the locations of fBSs are fixed and the mobility of fMSs are limited, if the CCI is caused by an mMS, the CFO, power, and delay values measured will be varying over time, whereas they will be fairly constant for an fBS, and displaying limited variations over time for an fMS. Hence, based on these three criteria, the fBS should be able to decide whether the source of CCI is an mMS or a femtocell.

To be able to track the changes in power and delay of a certain mMS, it is required to perform the corresponding measurements over multiple consecutive frames, where a frame is a certain number of adjacent symbols, for the same mMS. That means that the fBS needs to keep track of the subcarriers assigned to the same mMS over multiple frames. This can be achieved by building a chain of the clusters with close delay, power, and CFO values in adjacent frames, assuming that the delay, power, and CFO of an mMS cannot change sharply from one frame to another.

##### B. Hand-off Between Macrocell-BS and Femtocell-BS

In a co-channel femtocell implementation, delay and power measurements can be used to find the direction of movement of an mMS, e.g., it can be concluded that an mMS is moving away from the fBS when its delay is increasing, and its power level is decreasing.

Information about the direction of movement of mMSs can make the hand-off decisions between fBS and mBS more robust. Hand-off decisions solely based on power measurements can be misleading in case of strong fading, i.e., an instant fading in the signal power can trigger an unnecessary hand-off. However, if the decrease in power is supported by an increasing delay measurement, then the hand-off decision would be much more reliable.

Note that an fBS may also reschedule its own users to a different frequency band, if an mMS using a frequency band reused by the fBS moves closer to the fBS.

##### C. Causing CCI to the Minimum Number of mMSs Possible

In a macrocell system with reuse factor not equal to 1, adjacent cells will be using separate frequency bands. In a cellular system where reuse factor is equal to 3, a femtocell that is located in the middle of 3 mBSs will be detecting signals of all these macrocells. In this scenario, a co-channel femtocell would be expected to determine the occupancy of all three bands separately, and pick the band with the least occupancy to operate. However, if the occupancy rates of all 3 target bands are approximately the same, it would be reasonable that the fBS picks the band with the least number of users, which it can detect through user separation, so that the number of macrocell users affected by CCI is the smallest.

#### V. SIMULATION RESULTS

Computer simulations were performed in order to verify the relationship between  $c(\mathbf{r}_\tau, \mathbf{r}_\xi)$  and  $\sigma_{\xi_j}^2 / \sigma_{\tilde{\tau}_j}^2$ , and to test the performance of the proposed user separation algorithm. In the simulations, a WiMAX UL-PUSC system is considered and both an AWGN channel and a 6-tap multipath channel (ITU-R Vehicular A) are employed. Detailed simulation parameters are provided in Table-II, where RTD stands for the round-trip-delay.

In Fig. 3, the  $c(\mathbf{r}_\tau, \mathbf{r}_\xi)$  and  $\sigma_{\xi_j}^2 / \sigma_{\tilde{\tau}_j}^2$  ratios obtained at different received SNR levels are shown. The variances of the normalized estimators ( $\sigma_{\xi_j}^2$  and  $\sigma_{\tilde{\tau}_j}^2$ ) are the mean values of the variances found for each  $\xi_j$  and  $\tilde{\tau}_j$ . Note that the two ratios have very close values regardless of the SNR. Fig. 3 also shows the relationship between  $\sqrt{c(\mathbf{r}_\tau, \mathbf{r}_\xi)}$  and the optimum ratio of cluster dimensions ( $D_{\xi_j} / D_{\tilde{\tau}_j}$ ), which is determined performing an exhaustive search among possible values. The closeness of the corresponding values validates the relationship claimed in Section III.

Performance of the proposed algorithm was quantized via simulations using the following performance metrics:

TABLE II  
SIMULATION PARAMETERS

Parameter	Value
FFT Size	512
Occupied subcarriers	360
$N_{CP}$ , CP Duration	1/8, 11.2 $\mu s$
Number of users	10
Sampling frequency	5.714 MHz
Symbol Time	100.8 $\mu s$
Bandwidth	5 MHz
CFOs (in Hz)	[-500, -400, ..., 0, ..., 400, 500]
User distances (in m)	[100, 200, 400, 600, ..., 1800]
RTDs (in samples)	[4, 8, 15, 23, 30, 38, 46, 53, 61, 69]

TABLE III  
USER SEPARATION PERFORMANCES WHEN RECEIVED POWERS DEPEND  
ON USER DISTANCES

	<b>AWGN</b>	<b>MP</b>
$P_{N_u}$	86.07%	81.25%
$P_\Gamma$	78.55%	77.78%

Performance in finding the number of users:

$$P_{N_u} = 100 \times \left( 1 - \frac{|\hat{N}_u - N_u|}{N_u} \right) \quad (15)$$

Performance in finding the user subcarriers:

$$P_\Gamma = 100 \times \frac{\sum_{i,k} \delta_D(\hat{\Gamma}_i(k) - \Gamma_i(k))}{\sum_i N_i}, \quad (16)$$

where  $\delta_D$  is the Dirac delta function. The performances obtained for AWGN and MP channels are demonstrated in Fig. 4. The assumption in the corresponding simulations was that the received SNR is the same for all users regardless of their distance. The performance at each SNR is maximized by employing the optimum cluster dimension given by  $\sqrt{c(r_\tau, r_\xi)}$ . The results show that better than 90% user separation performance is achievable for sufficiently high SNR values.

In Table-III, additional simulation results are provided, where the received powers from different users depend on their distances to the receiver as specified in Table-II (free space path loss model is considered). The blocks whose power levels do not exceed a certain threshold are discarded as in (5). Simulation results in Table-III show that in average 80% accuracy is achievable in a practical scenario.

## VI. CONCLUDING REMARKS

Separation of UL-OFDMA user signals based on CFO and delay estimation is proposed. For all frequency allocation blocks that constitute an UL symbol, the estimations are performed. After normalization, the blocks are clustered

according to the estimated values. It is claimed that the ratio of cluster dimensions can be optimized utilizing the calculated variances of sets of correlation angles, and through practical simulations this claim is validated. Also, a rather high user separation performance is obtained, which proves the feasibility of the proposed algorithm.

## REFERENCES

- [1] M. Pun, M. Morelli, and C. Kuo, "Maximum-likelihood synchronization and channel estimation for OFDMA uplink transmissions," *IEEE Trans. Commun.*, vol. 54, no. 4, pp. 726–736, 2006.
- [2] Z. Cao, U. Tureli, and Y. Yao, "Deterministic multiuser carrier-frequency offset estimation for interleaved OFDMA uplink," *IEEE Trans. Commun.*, vol. 52, no. 9, pp. 1585–1594, 2004.
- [3] J. van de Beek, M. Sandell, and P. Borjesson, "ML estimation of time and frequency offset in OFDM systems," *IEEE Trans. Signal Process.*, vol. 45, no. 7, pp. 1800–1805, 1997.
- [4] M. Morelli, "Timing and frequency synchronization for the uplink of an OFDMA system," *IEEE Trans. Commun.*, vol. 52, no. 2, pp. 296–306, 2004.
- [5] R. Fantacci, D. Marabissi, and S. Papini, "Multiuser interference cancellation receivers for OFDMA uplink communications with carrier frequency offset," in *Proc. IEEE Global Telecommun. Conf. (GLOBECOM)*, vol. 5, Dallas, TX, Nov. 2004, pp. 2808–2812.
- [6] K. Kim, Y. Han, and S. Kim, "Joint subcarrier and power allocation in uplink OFDMA systems," *IEEE Commun. Lett.*, vol. 9, no. 6, pp. 526–528, 2005.
- [7] Z. Cao, U. Tureli, and Y. Yao, "User Separation and Frequency-Time Synchronization for the Uplink of Interleaved OFDMA," in *Proc. IEEE Asilomar Conf. on Signals, Systems and Computers*, vol. 2, Pacific Grove, CA, Nov. 2002, pp. 1842–1846.
- [8] P. Moose, "A technique for orthogonal frequency division multiplexing frequency offset correction," *IEEE Trans. Commun.*, vol. 42, no. 10, pp. 2908–2914, 1994.
- [9] M. E. Sahin, I. Guvenc, M. R. Jeong, and H. Arslan, "Opportunity detection for OFDMA systems with timing misalignment," in *Proc. IEEE Global Telecommun. Conf. (GLOBECOM)*, New Orleans, LA, Nov. 2008, pp. 1–6.
- [10] J. G. Andrews, A. Ghosh, and R. Muhamed, *Fundamentals of WiMAX: Understanding Broadband Wireless Networking*. Prentice-Hall, Feb. 2007.
- [11] S. Chiu, "Fuzzy model identification based on cluster estimation," *Intelligent and Fuzzy Systems*, vol. 2, no. 3, pp. 267–278, 1994.
- [12] R. Yager and D. Filev, "Generation of fuzzy rules by mountain clustering," *Intelligent and Fuzzy Systems*, vol. 2, no. 3, pp. 209–219, 1994.
- [13] G. Seber, *Multivariate Observations*. John Wiley & Sons, 1984.
- [14] H. Spath, *Cluster Dissection and Analysis: Theory, FORTRAN Programs, Examples*. Horwood New York: Halsted Press [distributor], Chichester, 1985.

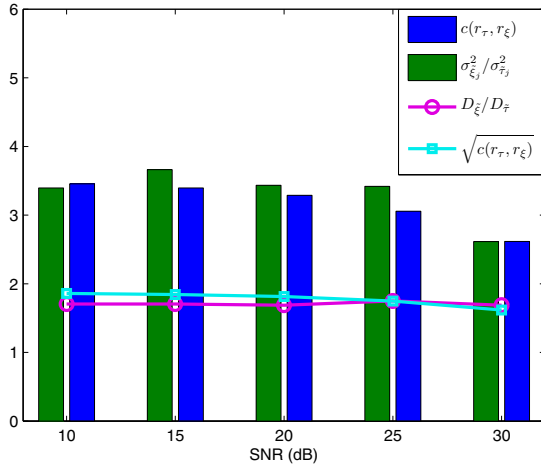


Fig. 3. Relationship between  $c(r_\tau, r_\xi)$  and  $\sigma_{\xi_j}^2 / \sigma_{\tau_j}^2$ , and the relationship between  $\sqrt{c(r_\tau, r_\xi)}$  and the optimum ratio of cluster dimensions ( $D_\xi / D_\tau$ ).

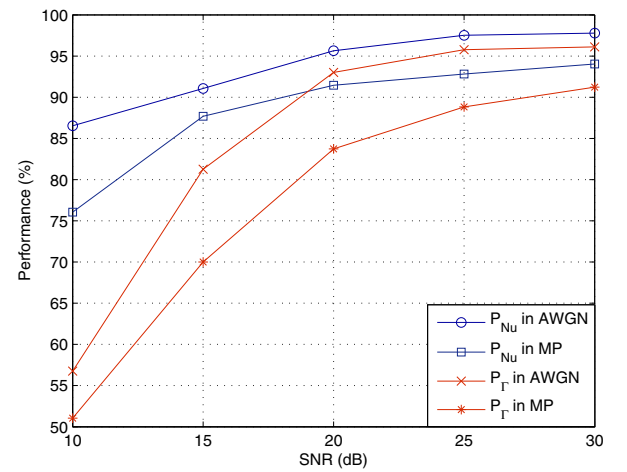


Fig. 4. Performances in finding the number of users and separating the user subcarriers in AWGN and MP channels assuming the same SNR for all users.